The influence of a weakening of the Atlantic meridional overturning circulation on ENSO

A. Timmermann[1], **Y. Okumura**[1], **S.-I. An**[2], **A. Clement**[3], **B. Dong**[4], **E. Guilyardi**[4,5], **A. Hu**[6] **J. H. Jungclaus**[7], **M. Renold**[8], **T.F. Stocker**[8], **R.J. Stouffer**[9], **R. Sutton**[4], **S.-P. Xie**[1], **J, Yin**[9]

[1] IPRC, SOEST, University of Hawaii, Honolulu, HI 96822, USA

[2] Dept. of Atmospheric Sciences, Yonsei University, Seoul, 120-749, Korea

[3] RSMAS/MPO, University of Miami, Miami, FL 33149, USA

[4] Department of Meteorology, University of Reading, Reading RG6 6BB, U.K

[5] IPSL/LOCEAN, Paris Cedex, France

[6] National Center for Atmospheric Research, P.O. Box 3000, Boulder, Colorado 80307, USA

[7] Max Planck Institute of Meteorology, 20146 Hamburg, Germany

[8] Climate and Environmental Physics, Physics Institute, University of Bern, Switzerland

[9] NOAA/Geophysical Fluid Dynamics Laboratory and Program in Atmospheric and Oceanic Sciences, Princeton University, Princeton, NJ, USA

Journal of Climate, submitted

February 8, 2007

Abstract

The influences of a substantial weakening of the Atlantic Meridional Overturning Circulation (AMOC) on the tropical Pacific climate mean state, the annual cycle and ENSO variability are studied using five different Coupled General Circulation Models (CGCMs). In the CGCMs a substantial weakening of the AMOC is induced by adding freshwater flux forcing in the northern North Atlantic. In response, the well-known surface temperature dipole in the low-latitude Atlantic establishes, which re-organizes the large-scale tropical atmospheric circulation by increasing the northeasterly trade winds. This leads to a southward shift of the Intertropical Convergence Zone (ITCZ) in the tropical Atlantic and also the eastern tropical Pacific. Due to evaporative fluxes, mixing and changes in Ekman divergence a meridional temperature anomaly is generated in the northeastern tropical Pacific which leads to the development of a meridionally symmetric thermal background state. In four out of five CGCMs this leads to a substantial weakening of the annual cycle in the eastern equatorial Pacific and a subsequent intensification of ENSO variability due to nonlinear interactions. In one of the CGCM simulations an ENSO intensification occurs as a result of a zonal mean thermocline

shoaling.

Our analysis suggests that the atmospheric circulation changes forced by tropical Atlantic SSTs can easily influence the large-scale atmospheric circulation and hence tropical eastern Pacific climate. Furthermore, we conclude that the existence of the present-day tropical Pacific cold tongue complex and the annual cycle in the eastern equatorial Pacific are partly controlled by the strength of the AMOC. The results may have important implications for the interpretation of global multidecadal variability and paleo-proxy data.

1. Introduction

Using Coupled General Circulation models it has been shown e.g. Manabe and Stouffer (1988); Delworth et al. (1993); Timmermann et al. (1998); Vellinga et al. (2001); Knutti et al. (2004); Timmermann et al. (2005a,b); Dahl et al. (2005); Zhang and Delworth (2005); Broccoli et al. (2006) that a weakening or a collapse of the Atlantic meridional overturning circulation generates substantial cooling in the North Atlantic, while leading to slightly warmer conditions in the South Atlantic. In turn an asymmetric meridional temperature seesaw is established which encompasses not only the tropical regions but also southern polar latitudes (Blunier et al. 1998; Stocker and Johnsen 2003) and the northern North Pacific. The tropical atmospheric response to this large-scale asymmetric meridional dipole is associated with an intensification of the northeasterly trade winds, pushing the Atlantic Intertropical Convergence Zone (ITCZ) southward as documented by paleo-proxy data (Peterson et al. 2000) and climate model simulations (Dong and Sutton 2002; Dahl et al. 2005; Zhang and Delworth 2005). This response helps to compensate for the heat loss in the North Atlantic (Broccoli et al. 2006). The ITCZ shift is brought about by anomalous temperature advection generated by anomalous northerly winds and by increased evaporation and latent cooling. The associated northern tropical Atlantic cooling in turn feeds back to the atmospheric circulation via boundary-layer responses and the linear baroclinic response

described in Gill (1980). This wind response feedback helps to amplify the cooling (warming) north (south) of the equator.

A large cooling in the northern tropical Atlantic (and in particular in the Caribbean) induces a large-scale anticyclonic circulation pattern (Xie et al. 2006), which is accompanied by a northerly trade wind intensification in the northeastern tropical Pacific. This trade wind response leads to a southward displacement of the Pacific ITCZ (Zhang and Delworth 2005) and the generation of a meridional SST anomaly (Dahl et al. 2005) due anomalous heat transports and the wind-evaporation SST (WES) feedback. These results highlight the importance of the atmospheric circulation to syncrhonize tropical Atlantic and Pacific climate anomalies on long timescales.

Another mechanism which was recently proposed (Hsieh and Bryan 1996; Huang et al. 2000; Goodman 2001; Cessi et al. 2004; Johnson and Marshall 2004; Timmermann et al. 2005a) to explain the synchronization between Atlantic and Pacific climate anomalies during a shutdown of the AMOC involves oceanic wave dynamics. Density anomalies in the northern North Atlantic trigger oceanic Kelvin waves which propagate southward along the American coast and subsequently along the equator. At the West African coast energy radiates as Rossby waves into the interior of the northern and southern basins. Wave energy reaches the Indian Ocean by Kelvin waves traveling around the southern tip of Africa. Passing the

Indonesian passages, the Kelvin waves eventually reach the Pacific Ocean. Through Rossby wave shedding in the Pacific the thermocline readjusts on timescale of decades. It was shown (Huang et al. 2000; Goodman 2001; Cessi et al. 2004; Timmermann et al. 2005a) that a shutdown of the AMOC may lead to a deepening of the equatorial thermocline in the eastern equatorial Pacific of 10-40m. This may be enough to weaken the amplitude of ENSO significantly (Timmermann et al. 2005a).

Using a coupled atmosphere-ocean model of intermediate complexity forced with a freshwater pulse in the northern North Atlantic, Timmermann et al. (2005a) showed that the thermocline anomalies in the Pacific associated with a substantial weakening of the AMOC may lead to a strong suppression of ENSO variability. However, as will be shown in our study here, the oceanic synchronization mechanisms may be overcompensated by the atmospheric bridge generated by Atlantic SST anomalies which also induces thermocline depth anomalies in the tropical and subtropical Pacific due to Ekman pumping. As will be shown here, through interactions with the annual cycle a shutdown of the AMOC may even generate an intensification of ENSO, on top of the purely oceanic ENSO suppression mechanism suggested in Timmermann et al. (2005a).

The focus of our study is the impact of an AMOC shutdown on the tropical mean climate in the Pacific, the annual cycle, ENSO and their interactions. Analysing water-hosing experiments recently performed with

five different state-of-the-art CGCMs we follow a conceptual framework for ENSO amplitude control outlined by Timmermann et al. (2006). As part of this framework it was proposed that changes of the meridional asymmetry in the eastern tropical Pacific (which can be modulated on long timescales e.g. by orbital forcing or by a shutdown of the AMOC) change the amplitude of the annual cycle in the eastern equatorial Pacific (Xie 1994). Due to the frequency-entrainment mechanism a weakened annual cycle may lead to an intensification of the ENSO amplitude and vice versa, (Chang et al. 1994; Liu 2002; Timmermann et al. 2006). Frequency entrainment is a part of the phase-synchronization process (Huygens 1669; Arnol'd 1965; Bak et al. 1985; Pikovsky et al. 2000) and is a common feature of periodically forced nonlinear oscillatory systems. Its presence is a clear manifestation of nonlinear dynamics.

The paper is organized as follows. After a brief description of the five different CGCMs used in this study and of the modeling experiments (section 2), an overview of the performance of the climate model simulations in the tropical Pacific and Atlantic is given in section 3. The global temperature and thermocline response to a shutdown of the AMOC will be studied in section 4. Section 5 addresses the question of how changes in the meridional asymmetry in the eastern tropical Pacific affect the strength of the annual cycle and ENSO. Simulated annual cycle-ENSO interactions will be described in section 6. Section 7 summarizes our main results and

section 8 discusses their main implications for the interpretation of multidecadal variability and for paleo-climate dynamics as well as for future greenhouse warming.

2. Model description and experimental design

As part of the CMIP model intercomparison project (Collins and the CMIP Modelling Groups 2005; Meehl et al. 2005) water-hosing experiments were conducted under pre-industrial or present-day climate conditions (Stouffer et al. 2006). Different CGCMs were forced with a step-function-like 100-year-long freshwater pulse which was applied to the northern North Atlantic (50°N-70°N). The response of the climate system to a pulse with an amplitude of 0.1 and 1 Sv has been described in detail in Stouffer et al. (2006). Some of the models used in our study such as the CCSM3 model do not follow exactly the CMIP waterhosing protocol.

The following model set-ups were used to study the influence of a substantial AMOC weakening on tropical Pacific climate:

GFDL CM2.1: The GFDL CM2.1 is a fully coupled atmosphere-ocean general circulation model developed at NOAA's Geophysical Fluid Dynamics Laboratory. The horizontal resolution of the atmospheric model and land model of GFDL CM2.1 is 2° latitude by 2.5° longitude. The at-

mospheric model has 24 vertical levels with the top at about 3 hPa. It employs a finite volume dynamical core and uses the pre-industrial radiative forcing condition of year 1860. The oceanic model is based on the GFDL MOM4 codes, which uses a tri-polar grid to avoid the North Pole singularity. The horizontal resolution is 1° in latitude and longitude with enhanced resolution in the meridional direction in the tropics. The meridional resolution at the equator is 1/3°. There are 50 vertical levels with 22 evenly spaced levels in the top 220 m. The water exchange across the ocean surface is represented in the model with a real water flux. A dynamical-thermodynamical sea ice model with the elastic-viscous-plastic technique to calculate internal ice stresses is used to predict the sea ice. The details of the model configurations, coupling procedure and performance can be found in Delworth and et al. (2006); Gnanadesikan and et al. (2006); Wittenberg and et al. (2006); Griffies and et al. (2006). The last 200 years of a multicentury pre-industrial model integration are chosen as the control run. In the water-hosing experiment, 1 Sv external freshwater flux is uniformly added into 50°-70°N of the North Atlantic for 100 years. Without a global compensation, this freshwater input would add about 9 m of globally averaged sea level over the hosing period. This model does not use any flux-adjustments.

NCAR CCSM2: The second model analysed here is the National Cen-

ter for Atmospheric Research's Community Climate System Model version 2.0 (Kiehl and Gent 2004). Its atmospheric component is the NCAR Community Atmospheric Model (CAM2) with T42 resolution and 26 levels vertically. The ocean model is a version of the Parallel Ocean Program (POP) developed at Los Alamos National Lab with 1 degree resolution and enhanced meridional resolution (1/2 degree) in the equatorial tropics, and with 40 vertical levels. The sea ice model is the Community Sea Ice Model (CSIM4) with elastic-viscous-plastic dynamics, a subgrid-scale thickness distribution, and energy conserving thermodynamics. The land model is the Community Land Model (CLM2). Although the ocean model is a free surface model, the virtual salt flux is used here for the air-sea freshwater exchanges. The present-day control simulation is integrated for 1000 years. Here only the model years 500-699 of the control simulation will be analyzed. The hosing experiment is branched from the control run at year 500. The 1 Sv additional freshwater flux is uniformly distributed in the northern North Atlantic between 50°N and 70°N without a global salinity compensation. Therefore, the global mean salinity is not conserved in this hosing experiment and the global mean sea-level remains constant.

NCAR CCSM3: The Community Climate System Model (CCSM, version 3.0), developed by the National Centre of Climate research (NCAR) is used in the low resolution version suitable for long term simulations

(Yeager et al. 2006). It is a comprehensive atmosphere-ocean general circulation/land surface model with a resolution of T31 in the atmosphere and a variable horizontal resolution in the ocean ranging from 3.75° x (1.8° to 0.9°) and increasing towards the tropics. The ocean model consists of 25 irregularly spaced levels with a relatively fine spacing in the upper ocean. All simulations conducted here refer to a control simulation under perpetual 1990 AD conditions (present-day climate set-up). The perturbation experiment consists of a strong "triangular" freshwater forcing history in the North Atlantic with freshwater being added between 50°N and 70°N. The freshwater forcing increases from 0 to 2 Sv for 100 years, and then decreases back to 0 Sv during another 100 years. The global salt balance is satisfied by uniformly removing freshwater from the remaining ocean surface.

MPI-OM1: The MPI-OM1 coupled model consists of the atmosphere/land component ECHAM5 (Roeckner et al. 2003) and the ocean/sea-ice model MPI-OM (Marsland et al. 2003). The configuration used here is a version of the IPCC-AR4 set-up described by Jungclaus et al. (2006). Jungclaus et al. (2006) also showed that an improved parameterization of the wind-stress calculation in a more recent version of the MPI model results in an improved simulation of the cold bias and the ENSO characteristics. The atmosphere is run at T31 spectral resolution with 19 hybrid levels and the

ocean grid has a resolution of 3° with grid poles moved to Greenland and Antarctica leading to grid sizes from 20 km near Greenland to 375 km in the Pacific. There is no refinement of the grid in the equatorial region. There are 40 unevenly spaced levels in the vertical. The model does not require flux adjustment to maintain a stable pre-industrial climate. The water-hosing experiment is started from year 150 of a 1000-year-long pre-industrial control integration by adding instantaneously to the atmospheric flux field, a fresh water flux of 1 Sv distributed over the North Atlantic between 50°N and 70°N. The fresh water flux is not compensated by extraction elsewhere (as to simulate the massive disintegration of ice sheets). The water-hosing is kept constant for 100 years. Thereafter the integration is continued for another 100 years allowing the MOC to recover.

UKMO HadCM3: HadCM3 is a coupled atmosphere-ocean GCM developed at the Hadley Centre and described by Gordon et al. (2000). It has a stable control climatology and does not use flux adjustments. The atmospheric component of the model has 19 levels with a horizontal resolution of 2.5 degrees of latitude by 3.75 degrees of longitude. The oceanic component of the model has 20 levels with a horizontal resolution of 1.25 x 1.25 degrees and employs a scheme to parameterize horizontal mixing of tracers with a variable thickness diffusion parameterization (Wright 1997). Near-surface vertical mixing is parameterized partly by a Kraus-

Turner mixed layer scheme for tracers (Kraus and Turner 1967), and a K-theory scheme (Pacanowski and Philander 1981) for momentum. The sea ice model uses a simple thermodynamic scheme including leads and snow-cover. Ice is advected by the surface ocean current only. The control run uses pre-industrial boundary conditions. The 1 Sv freshwater pulse is evenly distributed over the North Atlantic between 50°N and 70°N for 100 years. The freshwater hosing experiment is continued for another 100 years, without applying additional freshwater fluxes. These modeling experiments do not employ salinity compensation.

[Table 1 about here.]

3. Model performance of the control simulations

a. *Annual mean state and interannual variability*

A comparison of the simulated pre-industrial and present-day SST mean states for the five different models and the observations is shown in Figure 1. Generally the five different CGCMs simulate the tropical climate mean state and its interannual variability quite realistically[1]. However, there are several features some of these models fail to simulate correctly. As compared to the observations (OISST SST data Reynolds et al. (2002) and

[1]It should however be noted that some of the control simulations analyzed here represent pre-industrial conditions, rather than present-day conditions.

Kalnay and et al. (1996), wind stress), all of the CGCM control simulations are too cold in the western and central equatorial Pacific. This feature is most strongly pronounced in the MPI-OM1 control simulation. In this model the mean thermocline depth, as characterized here by the depth of the 20°C isotherm, is too shallow in the western tropical Pacific resulting in too large interannual variabilities throughout the entire tropical Pacific.

[Figure 1 about here.]

In addition to the typical equatorial cold bias, these model simulations exhibit a warm bias in the southeastern Pacific, which is most strongly pronounced in the CCSM2, CCSM3 and the HadCM3 model simulations, whereas it is weakest in the GFDL CM2.1 model. Different suggestions have been made to explain the warm biases in the upwelling regions, ranging from stratus-cloud representations (Philander et al. 1996; Yu and Mechoso 1999; Wang et al. 1999), missing Tsuchyia jets (J. McCreary, personal communication, 2006), lack of mesoscale variability (Seo et al. 2006) and overestimation of vertical mixing in coupled models (K. Richards, personal communication, 2006). This underestimated meridional asymmetry often leads to the development of an unrealistic double ITCZ in both hemispheres and to the generation of strong semi-annual cycles in the eastern equatorial Pacific (see Figure 2) such as in the CCSM2 and CCSM3 model runs. The reduced meridional cross-equatorial asymmetry also leads to a

damping of interannual variability in the south-eastern tropical Pacific as documented by the CCSM2, CCSM3 and the HadCM3 model simulations.

[Figure 2 about here.]

Typically the general representation of the cold tongue complex and the equatorial annual cycle in CGCMs also influences the fidelity of the model to simulate the position of the ITCZ and the South Pacific Convergence Zone (SPCZ), the equatorial annual cycle and ENSO (Fig. 1, right panel). A too shallow thermocline in the warm pool as simulated by the CCSM3 model leads to a variance maximum in the warm pool, in contrast to observations which shows a maximum of the ENSO variance in the eastern equatorial Pacific. In the CCSM2 model the pattern of maximum ENSO variance corresponds to the area occupied by the tropical Pacific cold tongue. Similar associations can be found for all CGCM simulations analyzed here. The differences between simulated and observed mean-state might also have an influence on the sensitivity of ENSO to climate perturbations, such as greenhouse warming or a collapse of of the AMOC.

Similar to the south-eastern Pacific warm bias, large differences between observations and all of the CGCMs can be found in the tropical Atlantic. None of these models simulates the observed zonal temperature gradient along the equator realistically. All CGCMs analyzed here exhibit too high temperatures in the eastern tropical Atlantic. Furthermore, as compared to the observations, the GFDL, the CCSM2 and the CCSM3 model simulations exhibit cold anomalies in the Caribbean which are likely to affect also the cold tongue in the tropical Pacific through at-

mospheric teleconnections, as will be shown in this study.

b. *Equatorial Pacific annual cycle*

One key element for the generation of the equatorial annual cycle is the northern position of the Intertropical Convergence Zone (ITCZ) and the attendant meridional temperature asymmetry around the equator, both of which are partly triggered by the land-sea contrasts in the eastern equatorial Pacific area (Philander et al. 1996) and maintained by air-sea interactions (Xie 1996). The SST asymmetry generates cross equatorial winds, which in turn cool the southern tropical eastern Pacific by increased evaporation, upwelling, mixing and cloud-radiative forcing. North of the equator however, the cross equatorial winds lead to a warming due to reduced evaporation (as compared to the meridionally symmetric state) and reduced mixing. This north-south temperature asymmetry is further amplified by the generation of low-level stratus clouds which form over the cold waters and lead to increased reflection of solar radiation. The north-south temperature difference in turn generates cross-equatorial winds as a result of the Gill-response (Gill 1980). Thanks to the positive air-sea feedbacks the annual mean ITCZ is kept north of the equator.

With the changing seasons, the north-south SST asymmetry changes as well as the strength of the cross-equatorial trade winds. This provides the seeding for the annual cycle of SST on the equator. However, as will

be shown below, the meridional asymmetry is also strongly controlled by the strength of the AMOC. In addition, coupled air-sea interactions (Xie 1994; Li and Philander 1996; Yu and Mechoso 1999) involving evaporative cooling, mixing, and stratus clouds generate a westward-propagating equatorial zonal mode with near-annual frequency that intensifies the annual wind forcing and in turn the westward-propagating equatorial annual cycle of SST. This positive feedback leads to the establishment of a coupled annual cycle in the eastern and central equatorial Pacific. Physical processes responsible for the generation of the annual cycle of SST in the eastern equatorial Pacific are thus somewhat distinct from those that govern the interannual mixed thermocline/SST ENSO mode.

These coupled mechanisms are documented for the observations in Figure 2 (upper left). Weakened trade winds in spring to the west of the maximum warming, initiate a westward-propagation of the warm water anomaly via reductions of mixing, upwelling, reduced solar insolation and evaporative cooling. In boreal fall this cycle reverses, driven by the southerly wind component which originates from the atmospheric response to off-equatorial SST anomalies. Figure 2 shows the observed present-day annual cycle of SST and wind-stress and sea level height (annual mean subtracted), and the simulated pre-industrial annual cycles for the GFDL CM2.1, the HadCM3, the MPI-OM1 models and the present-day annual cycle for the CCSM2, CCSM3 control simulations. The CGCMs

apparently have severe problems in reproducing the observed coupled annual cycle of SST and winds realistically. In contrast to the observations the CCSM2,3 models exhibit a strong semi-annual cycle in the eastern equatorial Pacific, owing to the weak mean meridional asymmetry in these model simulations. The phase of the annual cycle is somewhat unrealistic also in the GFDL and the HadCM3 model, exhibiting an early warming (GFDL CM2.1) or a delayed warming phase in the far eastern equatorial Pacific (HadCM3). While the CCSM3 model annual cycle of thermocline anomalies involves annual Kelvin wave pulses with magnitudes of up to 25m, the GFDL model exhibits semi-annual thermocline anomalies which seem basically unrelated to the SST anomalies. Thermocline anomalies in the MPI-OM1 and the CCSM2 model are rather small, supporting the notion that the annual cycle of SST in the eastern equatorial Pacific does not primarily involve thermocline dynamics (Xie 1994). The thermocline anomalies in the HadCM3 model do not show any clear propagation and their relationship to the winds and SST anomalies is also more complex than for the other CGCMs. Disentangling the annual cycle of the thermocline depth anomalies in terms of wave reflection, off equatorial Ekman pumping and other processes (Wang et al. 2000) is beyond the scope of this paper.

4. Global response to AMOC shutdown

The time evolution of the maximum of the meridional streamfunction in the North Atlantic for the five different models is depicted in Figure 3. For each model 200 years of the control simulation are displayed (blue curves) and 200 years of the freshwater hosing experiment (red). The longterm mean strength of the AMOC in the control simulations varies between 15 and 22 Sv. In all simulations the strength of the AMOC drops down to 2.5-6 Sv shortly after the onset of the freshwater pulse. The strongly weakened AMOC state will be referred to as the *perturbation state*. The typical timescale for the shutdown of the AMOC is about 20-50 years, except for CCSM3 which was forced by a linearly increasing and decreasing freshwater flux, suggesting that wave-adjustment processes (Johnson and Marshall 2004) play an important role as well as advective processes (Goodman 2001).

[Figure 3 about here.]

Figure 4 shows the Atlantic and Pacific SST anomaly pattern associated with a perturbation state of the AMOC (averaged difference over the first 100 years of the perturbation state and the first 100 years of the control simulation) as simulated by the 5 CGCMs. We observe the well-known inter-hemispheric seesaw pattern in SST (Stocker and Johnsen 2003; Knutti et al. 2004), although the simulated temperature anomalies around Antarc-

tica are quite small, except for the HadCM3 and the CCSM3 response.

Large positive temperature anomalies can be found in the Benguela current region and can be partly explained in terms of a substantial weakening of the southerly along-shore winds in this area (Figure 4) which under unperturbed conditions pump cold waters to the surface.

[Figure 4 about here.]

Based on the robustness of these results, we can argue that the Benguela current region might be an optimal site to retrieve proxy records capturing the bipolar seesaw. Analyzing the time-evolution of these anomalies more in detail (not shown here) reveals that the cooling starts in the northern North Atlantic and spreads further south within a few decades until it reaches its full magnitude (typically 50 years after the beginning of the meltwater pulse). This spreading, which will be studied in more detail in a forthcoming study involves atmosphere-ocean interactions (Chiang and Bitz 2005), ocean dynamics and the adjustment of the Hadley circulation (Broccoli et al. 2006). While the adjustment mechanisms are robust in different models, what appears to be fundamental is the requirement for the atmosphere to transport heat into the cooler hemisphere as described by (Broccoli et al. 2006).

Figure 4 shows also a significant warming of up to 1°C in the tropical south-eastern Pacific, as well as a cooling of the tropical north-eastern Pacific by 2°C, consistent with the findings of Zhang and Delworth (2005);

Timmermann et al. (2005b). In the GFDL, the CCSM2,3 and the HADCM3 models this pattern is quite distinct from a zonal mode pattern sometimes referred to as a permanent El Niño state. In these model simulations one of the most striking features of the SSTA pattern in the tropical Pacific is the strong meridional structure near the equator which – superimposed on a meridionally asymmetric mean state of opposite direction – reduces the mean meridional asymmetry across the equator (see Figure 4). Eventually, during the shutdown phase the warm northeastern tropical Pacific cools, whereas the southeastern Pacific cold tongue complex warms substantially. During the mature shutdown phase, the Pacific temperature gradient across the equator is even reversed in some of the models, leading to a reversal of the mean cross-equatorial trade wind direction (see Figure 4) and also to a shift of the mean ITCZ to the southern hemisphere in some cases. This clearly illustrates that the position of the present-day annual mean ITCZ in these models is not only determined by continental asymmetries and air-sea interactions (Philander et al. 1996) but also by the presence or absence of an AMOC in the Atlantic ocean (Zhang and Delworth 2005) and the Atlantic-Pacific atmospheric bridge via Central America.

Four out the five CGCMs analysed here produce a rather consistent picture of changes in the eastern tropical Pacific which projects strongly onto a meridional mode pattern. The simulated tropical Pacific response

of the MPI-OM1 model is qualitatively very different. A substantial weakening of the AMOC in the MPI-OM1 model generates a permanent La Niña-like pattern (zonal mode) with only weak meridional mode contributions. This will have repercussions also on the sensitivity of the annual cycle and ENSO in this model, as will be shown below.

Atmospheric teleconnections from the tropical Atlantic play a crucial role in generating oceanic and atmospheric anomalies in the eastern tropical Pacific (Dong and Sutton 2002; Zhang and Delworth 2005). In response to the anomalous southward SST gradient in the tropical Atlantic, the Atlantic ITCZ shifts to the south (Fig. 4), forcing westward-propagating atmospheric Rossby waves. The Caribbean cooling and the associated increase in sea-level pressure are particularly important in communicating the Atlantic changes to the Pacific across a narrow land corridor of Central America: the intensified northeasterly trades blow over the tropical north-eastern Pacific, advecting cold, dry air and enhancing evaporation from the sea surface (Wu et al. 2005). The resultant cooling of the tropical north-eastern Pacific will trigger the WES feedback within the Pacific basin, amplifying the southward shift of the Pacific ITCZ and the corresponding warming in the tropical south-eastern Pacific. Air-sea interactions may further spread the equatorially-asymmetric anomalies to the west (Xie 1996).

While during the AMOC shutdown stages the thermocline anomalies in the Atlantic exhibit a rather model-independent structure (not shown) with shoaling in the tropical North Atlantic, largely due to surface cooling, a deepening in the southeastern Atlantic and the Benguela region, the equatorial Pacific response is less robust (see Figure 5).

[Figure 5 about here.]

Near the equator it is useful to split the simulated thermocline anomalies conceptually into a zonal mean and a zonal tilt term. In both, the CCSM2 and CCSM3 models the zonal mean equatorial thermocline[2] deepens by several meters. The vertical resoltion of the ocean general circulation models might also be an important factor in determining the exact value of the zonal mean thermocline changes. In general, the zonal mean thermocline depth is strongly controled by the eastern and western boundary fluxes and the zonally averaged meridional mass flux divergence. The zonally averaged meridional velocity can be obtained from the changes of the western boundary currents as well as the zonally averaged Sverdrup transport which in turn is driven by the wind-stress curl. For reasons of simplification we will focus here on the effect of the Sverdrup transport. The zonal and temporal mean thermocline depth changes in the waterhosing experiments are partly controled by the curvature changes of the wind-stress, involving the second order meridional derivative. In fact the deep-

[2]taken here as the depth of the 20°C isotherm averaged between 120°E and 90°W

ening of the zonal mean thermocline in the CCSM2 and CCSM3 model goes along with zonal mean Sverdrup transport convergence (not shown) towards the equator. In the MPI-OM1 and the HadCM3 model the zonal mean thermocline shoals by 8m and 4m, respectively. This zonal mean shoaling is accompanied by a Sverdrup transport divergence (not shown). The GFDL model simulates a zonal mean thermocline shoaling of 4m, in spite of a Sverdrup transport convergence. In general, these diagnosed relationships have to be interpreted carefully. We have identified here the zonally integrated mass-flux into the equatorial thermocline as the zonal intregal of the Sverdrup transport convergence, neglecting changes of the Indonesian throughflow and the fact that the Sverdrup transport is a barotropic transport, rather than a near-surface transport into the thermocline. The large model discrepancies in the simulated zonal mean thermocline depth anomalies can be partly attributed to the fact that even small meridional changes in the position of the wind-stress pattern can lead to large changes of the curvature of the wind stress.

The anomalous zonal thermocline gradients on the equator (Figure 5) can be related to the zonal wind-stress changes induced by the AMOC weakening. It can be clearly seen that negative near-equatorial wind-stress anomalies in the CCSM2 and CCSM3 model lead to a deepening of the thermocline anomaly towards the west. The large positive wind-stress anomalies west of 150°W simulated in the HadCM3 and the GFDL

model lead to a shoaling of the thermocline towards the west.

We can summarize that in all CGCMs, except for the MPI model the eastern equatorial Pacific is deeper during the AMOC perturbation state than under control run conditions. This effect would lead to a weakening of the efficiency of the thermocline feedback, which normally plays an essential role in amplifying ENSO variability. On the other hand three (GFDL, MPI and HadCM) out of five models exhibit a zonal mean thermocline shoaling which might help to amplify ENSO variability (Zebiak and Cane 1987).

5. Effect of background state changes on annual cycle and ENSO

Based on the mechanisms which govern the strength of the present-day annual cycle we expect that a weakening of the meridional asymmetry in the eastern tropical Pacific, such as the one diagnosed in four out of the five CGCM simulations (Figure 4) will lead to a weakening of the strength of the annual cycle. This behavior is in fact simulated by the CGCM simulations as revealed by the power spectra of the simulated Niño 3 SST time series shown in Figure 6.

[Figure 6 about here.]

As a result of the AMOC weakening, the strength of the annual cycle reduces substantially in four of the five models (CCSM2,3, GFDL 2.1 and HADCM3). This result supports the notion that the strength of the annual cycle in the eastern tropical Pacific is to a large extent controlled by cross-equatorial winds, which are driven by the meridional SST asymmetry in the eastern equatorial Pacific (Xie 1994) and remotely by the SST conditions in the tropical Atlantic.

To understand the mechanisms for the reduction of the equatorial Pacific annual cycle in four of the five CGCM waterhosing experiments analysed here, we computed the anomalous seasonal cycle of SST, thermocline depth and wind stress (see Figure 7).

[Figure 7 about here.]

Although the mean unperturbed seasonal cycle of the thermocline depth appears unrelated to that of the SST in the control simulations, the anomalous thermocline changes during the waterhosing phase show a clear tendency to be accompanied by temperature anomalies of the same sign.

Anomalous fall to winter cooling near the equator leads to a weak intensification of the annual cycle amplitude in the MPI-OM1 model. There is evidence for an eastward propagating upwelling Kelvin wave, which is generated by anomalous equatorial easterlies in September. This upwelling signal is likely to influence the SST in fall-to winter, thereby amplifying the mean annual cycle (figure 2). This works particularly well, be-

cause the annual mean thermocline anomaly in the MPI model is already shallower during the waterhosing experiment than in the control run (see Figure 5). The boreal summer warming around 120°-100°W is probably due to surface processes and in particular due to a reduction of the wind strength in May, rather than due to ocean dynamical processes.

All other CGCMs exhibit a summer to winter warming and spring-time cooling, which is opposite to the mean annual cycle of SST and wind-stress. In comparison to the MPI-OM1 perturbation experiment, the other four CGCMs simulate a deeper mean thermocline in the eastern equatorial Pacific. Thermocline depth changes triggered by wind-stress changes (see GFDL and NCAR models) are not very efficient in modulating the SST due to a weakened thermocline feedback. This leads to an overall lower sensitivity. Spring time cooling in these models is an important contributor to a weakening of the equatorial annual cycle and is induced by strong annual mean northeasterly off-equatorial trade winds associated with a Caribbean positive sea level pressure anomaly and the seasonal modulation of the air-sea coupling strength in the northeastern Pacific, which partly relates to the seasonal cycle of the mean thermocline depth. In fact, such a boreal spring cooling in the eastern equatorial Pacific is also simulated in a regional coupled model of the eastern tropical Pacific in response to a 2°C decrease in tropical North Atlantic SST (Xie et al. 2006).

The power spectra in Figure 6 clearly show that in all 5 models ENSO variability is significantly enhanced during the waterhosing phase. One important controling factor for the amplitude of ENSO is the annual mean background state climate (thermocline depth, mean SST, zonal winds, coupling strength etc.) (Zebiak and Cane 1987). Another mechanism is ENSO's interaction with the annual cycle through the nonlinear frequency entrainment process described in Liu (2002); Timmermann et al. (2006).

As documented in Figure 5, the zonal mean equatorial thermocline depth averaged from 120°E and 90°W shoals in the GFDL, HadCM3 and the MPI-OM1 model by 4m, 3.7m, and 8m, respectively. According to idealized modeling studies (Fedorov and Philander 2000) such a thermocline shoaling might lead to an increase of ENSO instability for those models which exhibit a rather shallow zonal mean thermocline. In our case, only the MPI-OM1 model has a very shallow zonal mean thermocline (90 m) and the ENSO intensification in this model can be readily explained in terms of the linear theory of Fedorov and Philander (2000). Both, the GFDL and HadCM3 models on the other hand have a rather deep zonal mean thermocline (125-130m) and strong zonal mean winds. Their thermocline depth anomaly pattern under waterhosing conditions is associated with a reduction of the mean thermocline tilt. The linear theory of Fedorov and Philander (2000) is not directly applicable to this situation. Furthermore, the results of Fedorov and Philander (2000) are based on a two-strip model

which is not capable of capturing the effect of meridional thermocline and wind asymmetries.

To quantify the effect of the spatially inhomogenous thermocline, temperature and wind anomalies (annual mean and anomalous seasonal cycle changes) on the ENSO variance in more detail a series of sensitivity experiments using an intermediate anomaly-coupled ENSO model (Zebiak and Cane 1987) (ZC model) is conducted. The ocean model uses a 1.5 layer reduced gravity model, a surface layer model capturing frictional processes and the Ekman layer and an equation for the mixed layer temperature anomalies. The atmospheric model solves the first baroclinic mode equations on an equatorial beta-plane (Gill 1980) iteratively. The iterative procedure generates some atmospheric noise and subsequently ENSO irregularity. The intermediate model is used in the anomaly coupling mode, i.e. prognostic equations are solved for the anomaly with respect to a given annual mean background state – in our case the observational background state for the currents, the mean thermocline depth, the mean temperature and the winds plus an additional perturbation capturing the effect of an AMOC weakening on the tropical climate.

To obtain the background state perturbations, we used the tropical Pacific SST difference (Figure 4) between the AMOC perturbation state in the NCAR CCSM2 model and the control state as a forcing for the ZC model. Subsequently surface wind and wind divergence background state

anomalies are computed from the coupled intermediate model. These surface winds are used to force the 1.5 layer ocean model to calculate the surface-layer currents, upwelling and thermocline depth. Eventually, the diagnosed anomalies for SST and the computed anomalies for surface wind, surface wind divergence, surface layer currents, upwelling velocity, and thermocline height anomalies are added onto the observational present-day background state of the ZC model. This procedure has been done for the annual mean background state change (ANNM) in the tropical Pacific corresponding to a collapsed AMOC state, as well as for the anomalous annual cycle (ACY). A multi-century simulation is performed with the ZC model adding the background state perturbations ANNM and/or ACY to the observed present-day seasonally varying background state. Figure 8 shows the standard deviation of the Niño 3 SSTA simulated by the ZC model for the present-day control state, for the ANNM simulation, capturing the annual mean background state change of the CCSM2 model, the ACY experiment and the ANNM+ACY (ALL) experiment.

[Figure 8 about here.]

The annual mean background state changes (ANNM) lead to a weakening – and actually a shutdown – of ENSO activity (Figure 8), in consistency with the results of Timmermann et al. (2005a). This can be mostly attributed to the overall zonal mean thermocline deepening simulated by CCSM2 simulation (see Figure 5) as well as to changes of the meridional

advection of heat due to the symmetric SST structure (Figure 3). Apparently the annual mean background state changes cannot explain the observed ENSO intensification observed in the CCSM2 model (Figure 6). However, the annual cycle background state changes (ACY) lead to an intensification of ENSO variability in the intermediate ENSO model, in consistency with the results shown in Figure 6. Figures 6,7 clearly show that in the CCSM2 model the annual cycle strength due to the AMOC collapse reduces substantially. Hence, we can conclude from this intermediate model experiments that a weakening of the annual cycle background state forcing might be an important mechanism to intensify ENSO variability.

To understand the effect of the more dipolar thermocline anomaly structure simulated e.g. by the HadCM3 model (Figure 5) on ENSO in a more quantitative way, we perturbed the ZC model thermocline depth background state directly by the annual mean (HADCM3 ANNM) and/or seasonal cycle change (HADCM3 ACY) of the tropical thermocline depth field diagnosed from the HadCM3 waterhosing and control simulation. Figure 7 clearly reveals that the anomalous annual cycle projecting on an overall weakening of the mean annual cycle of thermocline depth is a booster for ENSO variability, whereas the annual mean change of the thermocline which is characterized by a deepening in the east and a shoaling in the west (Figure 5) leads to a reduction of ENSO. Both effects together

(HADCM3 ALL) can explain a net amplification of ENSO, as compared to ZC control simulation.

Based on our intermediate model simulations using the Zebiak and Cane (1987) intermediate ENSO model we can conclude that the zonal mean equatorial thermocline deepening as simulated by the CCSM2 and CCSM3 models, as well as the decrease in thermocline tilt simulated by the HadCM3 and GFDL CM2.1 model lead to a weakening of ENSO variability – in contrast to Figure 6. While the MPI-OM1 thermocline shoaling in the entire cold-tongue can explain the ENSO intensification in a linear framework (Fedorov and Philander 2000), other nonlinear mechanisms involving the annual cycle need to be invoked to explain the ENSO intensification in the CCSM2,3, the GFDL CM2.1 and the HadCM3 models.

6. Effect of annual cycle changes on ENSO

Here we focus on the four different models (GFDL CM2.1, CCSM2, CCSM3, HadCM3) which exhibit a weakening of the annual cycle and an accompanying intensification of ENSO amplitude during the collapsed AMOC period.

Under present-day conditions the seasonal dependence of the equatorial air-sea coupling strength is an important modulator for ENSO activity (Zebiak and Cane 1987; Tziperman et al. 1997). The coupling strength

is controlled by many different factors which include both atmospheric and oceanic processes. In boreal spring, the ITCZ is close to the equator which leads to large convergent and upward motion of air, heating the atmosphere via latent heating and moisture condensation. Interannual anomalies in this season will hence experience an enhanced Bjerknes feedback. On the other hand, zonal SST gradients as well as equatorial upwelling are relatively weak, thereby resulting in less efficient zonal and vertical advection in the equatorial ocean, respectively. As can be seen from Figure 2 (upper left panel), during the spring season the equatorial thermocline is shallower which might lead to an enhancement of the thermocline feedback (Galanti et al. 2002), thereby enhancing the effect of a wind-stress anomaly on the SST. The seasonal competition between the thermocline outcropping feedback and the wind-convergence feedback is quite delicate. Small shifts in the background state can lead to significant changes of the seasonality of the air-sea coupling strength. Other effects on the coupling strength which are neglected here are changes of the thermocline sharpness (Timmermann et al. 1999a) and changes in the interaction between intraseasonal wind noise and ENSO (Eisenman et al. 2005; Jin et al. 2006).

To diagnose changes of the air-sea coupling strength due to the weakened AMOC state, we diagnosed the atmospheric sensitivity (Timmermann et al. 1999a) from the monthly-stratified regression between zonal

wind-stress averaged over the central Pacific (170°E-140°W) and the Niño 3 SSTA[3]. The results are depicted in Figure 9.

[Figure 9 about here.]

For clarity we just focus on the CCSM2 and CCSM3 models. In both models an increase of the summer coupling atmospheric sensitivity can be observed which is accompanied by a variance increase of the simulated eastern equatorial Pacific temperatures in boreal winter. During the AMOC perturbation state interannual anomalies can grow faster during summer, leading to larger mature El Niño or La Niña events in winter. While similar features can be observed (not shown) also for the GFDL model, the variance changes in the HadCM3 model happen throughout the year (not shown) without considerable changes of the atmospheric sensitivity.

Attempts to understand why the summer air-sea coupling strength is enhanced for the weakened AMOC state were hampered by the fact that the seasonal modulation of the sensitivity is determined by the wind-convergence feedback, the thermocline outcropping nonlinearity and the strength of zonal and vertical SST gradients as well as other factors. Our analysis of the wind-convergence feedback (Zebiak and Cane 1987) (not shown) has revealed that the GFDL, CCSM2 and CCSM3 models simulate an enhanced spring to summer wind-divergence near the equator, which

[3]Here the assumption is made that the main response patterns in the tropical Pacific remain stable.

would in fact weaken the air-sea coupling strength in contrast to Figure 9. On the other hand these models simulate a shallower eastern equatorial thermocline during the boreal spring to summer (Figure 7), which might lead to an enhancement of the air-sea coupling trough an increased efficiency of the thermocline feedback. A more in-depth analysis of these feedbacks is very complicated and exceeds the scope of our paper.

As mentioned in the introduction there is ample evidence from CGCM simulations (Guilyardi 2005; Timmermann et al. 2006) as well as from observations (Gu and Philander 1995) that the strength of ENSO can be anti-correlated with the strength of the annual cycle in the eastern equatorial Pacific. This can be interpreted in terms of the nonlinear frequency entrainment concept described in Bak et al. (1985); Chang et al. (1994); Liu (2002). The main idea is that ENSO is a nonlinear oscillator which is periodically forced by the annual cycle in the eastern equatorial Pacific with a frequency that is incommensurate with its own eigenfrequency. For a weak annual cycle, ENSO maintains its eigenfrequency, whereas for a very strong annual cycle, ENSO's frequency is completely entrained into the forcing frequency and the interannual variance drops (Liu 2002). For a moderate annual cycle strength nonlinear resonances between ENSO and the annual cycle can occur in which ENSO frequency may become a rational multiple of the annual cycle frequency. Near certain thresholds, the selection of a single frequency may become more and more difficult and

ENSO can jump between different nonlinear resonances, possibly generating chaotic vacillations. This can be achieved either via the period-doubling bifurcation route to chaos (Chang et al. 1994) or through the quasi-periodic route to chaos (Tziperman et al. 1994). To adopt these types of idealized concepts to the tropical Pacific we have to note however, that the true forcing is the equatorial semi-annual and the off-equatorial top-of-the-atmosphere insolation. The annual cycle of winds is already a result of tropical air-sea interactions and can respond to interannual variability as well as the other way round, thereby complicating the interpretation.

Clearly, more work needs to be done to understand the interaction between the annual cycle and ENSO both in observations and CGCMs in more physical terms.

7. Summary

Our statistical analysis of the CGCM waterhosing simulations focused on five different CGCMs (GFDL CM2.1, NCAR CCSM2, NCAR CCSM3, MPI-OM1, UKMO HadCM3). In all of these model simulations, a collapse of the AMOC generates the Atlantic seesaw pattern of SSTA which triggers a large-scale atmospheric response. This atmospheric response is associated with an intensification of the northern hemispheric trade winds in the Atlantic, a large anomalous anti-cyclonic surface circulation in the

Caribbean and its surroundings, as well as a southward displacement of the ITCZ. Partly through the positive WES feedback, partly through large-scale changes of the meridional heat transport a negative SSTA is generated in the northern tropical Atlantic, whereas the southern Atlantic experiences a warming. This meridional asymmetry weakens the trade winds further (Gill 1980), thereby contributing to the positive WES-feedback. Although the South American continent is shielding somewhat the transmission of atmospheric anomalies from the Atlantic to the tropical Pacific, wind-anomalies can easily cross Central America, thereby triggering SST anomalies in the north-eastern tropical Pacific.

Furthermore, the large-scale cooling in the northern Pacific is also contributing to an overall strengthening of the Hadley cell and a trade wind intensification which can result in a southward displacement of the ITCZ in the Pacific and further cooling of the northeastern tropical Atlantic. Due to a southward shift of the Pacific ITCZ, consistently simulated in all of the CGCM waterhosing experiments analysed here, the southeastern tropical Pacific is warming. Ultimately, a reduced meridional asymmetry is established which leads to a weakening of the annual cycle in the case of the GFDL, the CCSM2, CCSM3 and HadCM3 models. Here we concluded that the weakening of the tropical Pacific annual cycle in the GFDL, UKMO and NCAR models most likely causes an intensification of ENSO. This behavior is reminiscent of the frequency entrainment mechanism and re-

lates to enhanced boreal summer air-sea instability. For these models linear instability arguments (Fedorov and Philander 2000) are unsuitable to explain the diagnosed ENSO intensification. In the MPI model a significant zonal mean thermocline shoaling of about 5-20 m is simulated, which leads to an intensification of the annual cycle in the eastern Pacific and of ENSO in accordance with linear theory. This indicates that the frequency-entrainment concept adopted here to explain the ENSO behavior of the other models is not a universal scenario but strongly depends on the existing background conditions changes and in particular of the simulated the thermocline depth anomalies.

A summary sketch of the diagnosed processes leading to an ENSO intensification during an AMOC collapse is depicted in Figure 10.

[Figure 10 about here.]

‘

8. Discussion

The results of this study may be relevant also for our understanding the multidecadal variability of ENSO activity during the twentieth century. Dong et al. (2006) present evidence that variations in SST associated with the Atlantic Multidecadal Oscillation (AMO, e.g. (Kerr 2000)) can modulate ENSO activity. The AMO, which is thought to be related to multi-

decadal fluctuations of the AMOC (e.g., Delworth and Mann (2000)), was in a negative phase from the mid-1960s to the 1990s, characterized by an anomalously cold North Atlantic and warm South Atlantic, and this period was associated with strong ENSO variability (see Figure 11) and a reduced annual cycle of SST in the eastern tropical Pacific.

[Figure 11 about here.]

The positive phase of the AMO from the mid 1930s to the late 1960s was associated with an intensified annual cycle and weak ENSO variability (Figure 11). The observational finding is consistent with our main hypothesis that multidecadal changes in the North Atlantic temperature modulate both the annual cycle and ENSO in the tropical Pacific.

Dong et al. (2006) reproduced the relationship between ENSO and the AMO qualitatively in idealized regional coupled experiments where Atlantic SSTs were prescribed to simulate positive and negative phases of the AMO, suggesting that ENSO activity is sensitive to changes in the AMOC. The multi-model results presented in our study are (with the exception of MPI-OM1) in that sense consistent with the results of Dong et al. (2006). Dong et al. (2006) suggest that thermocline eastward propagating thermocline anomalies play an important role in modulating ENSO activity on multidecadal timescales. This hypothesis is not directly confirmed by the analysis of the HadCM3 waterhosing experiment. While the anomalous seasonal cycle of thermocline depth anomalies shoals in boreal spring (Fig-

ure 7), the absolute thermocline depth anomaly does not change compared to the contol simulation. Furthermore the SST/thermocline as well as the wind-stress/SST sensitivities, both contributing to the coupling strength do not change significantly as a result of the AMOC perturbation.

It should be noted here that tropical Atlantic SST variations associated with the AMO are much smaller (typically in the order of 0.3°C) than those associated with a near-collapse of the AMOC (typically in the order of 3-6°C) (see Figure 4). Given that in both cases we observe a significant change of the ENSO variance, the question can be raised whether the simulated tropical Pacific response to tropical Atlantic forcing is perhaps strongly underestimated. Analysing the co-variability of ENSO and the AMO in CGCMs on multidecadal timescales will help to interpret the short observational record with more confidence. In fact, recent CGCM studies have found that the periodicity of simulated interdecadal "ENSO" amplitude modulations is similar to that of the simulated meridional overturning variations in the North Atlantic (Knutson et al. 1997; Timmermann et al. 1999b; Timmermann 2003).

The potential predictability of the strength of the Atlantic meridional overturning circulation on timescales of a few years to decades (Griffies and Bryan 1997; Grötzner et al. 1999; Latif et al. 2006) might also translate into a potential longterm predictability of the amplitude of the ENSO mode. This would be a type of regime-predictability (predictability of the

probability distribution of ENSO or of its higher order statistical moments) (Timmermann and Jin 2006), which may have many very interesting societal implications.

Black et al. (1999) reported evidence that multidecadal variations of the interhemispheric SST contrast in the Atlantic have an influence on riverine input into the Cariaco Basin, thereby supporting the proposed link between the AMO and the position of the Atlantic ITCZ on multidecadal timescales. Furthermore, on millennial timescales the hydrological paleo-proxy reconstructions from the Cariaco Basin (Lea et al. 2003), the Indian ocean (Ivanochko et al. 2005), from the western tropical Pacific (Stott et al. 2002) and the eastern tropical Pacific (Koutavas and Lynch-Stieglitz 2004) indicate that the ITCZ was displaced southward during the Heinrich events in the northern North Atlantic. Heinrich events are believed to represent glacial ice-sheet instabilities which have triggered major re-organizations of the AMOC (Hemming 2004). Paleo-evidence for our hypothesis controlling changes of the annual cycle and ENSO might come from fossil corals which lived during Heinrich events and which capture interannual variability associated with ENSO (Corrège et al. 2000; Tudhope et al. 2001). In such records the ratio between recorded interannual variability and the annual cycle strength might be an important indicator for the frequency-entrainment mechanism outlined here. Paleo evidence for enhanced decadal to interdecadal variability in the south-eastern

Pacific was recently reported using high resolution cores from off the coast of Peru during the period 12-10 ka B.P. (the Younger Dryas) and the Heinrich event I (see Figure 9, Rein et al. (2005)). It should however be noted that the estimated variance changes of this record need to be normalized by the sedimentation rate. The findings of Rein et al. (2005) are indicative of changes of the eastern tropical variability during major reorganizations of the AMOC. Whether the inferences from Rein et al. (2005) can be adopted to interpret ENSO changes during collapsed AMOC states still remains to be shown. Furthermore, the effect of orbitally-driven insolation changes on ENSO (Clement et al. 1999; Timmermann et al. 2006) might further complicate the interpretation of high-resolution tropical records.

The impact of an anticipated anthropogenic greenhouse warming on the AMOC has been the subject of many studies, e.g. Dixon et al. (1999). Most recent CGCM studies (Gregory and et al. 2005; Schmittner et al. 2005) suggest that a doubling of atmospheric CO_2 might lead to a weakening of the strength of the meridional overturning in the North Atlantic by 10% to 50%. According to our study a 50% decrease might already lead to substantial changes of the meridional temperature gradient in the eastern equatorial Pacific and hence to changes of the annual cycle and ENSO. However, it should also be noted that there are other processes internal to the Pacific which modulate the amplitude of ENSO under greenhouse warming conditions, such as changes of the thermocline sharp-

ness, westerly-wind burst activity, air-sea coupling and zonal thermocline gradients. Recent assessments of these internal Pacific effects in multi-model ensembles reveal that the ENSO response to greenhouse warming is highly model-dependent (Guilyardi 2005; Philip and van Oldenborgh 2006; Merryfield 2006).

The water-hosing experiments made a good case that the AMOC is an important factor for establishing the meridional asymmetry in Pacific/Atlantic climate. However, the AMOC is probably not the only factor; many TOGA-forced coupled models still have problems in keeping the Pacific ITCZ north of the equator even though observed SST is prescribed outside the tropical Pacific. The shape and topography of the continents and air-sea interactions are still important (Philander et al. 1996). Because latitudinal asymmetry is weak to begin with in some CGCMs, an AMOC shutdown may be enough to destroy this weak asymmetry, as shown here. In reality, the initial climatic asymmetry in the Pacific and Atlantic maybe much stronger and probably harder to reverse.

As documented by a recent analysis of CMIP water hosing experiments (Stouffer et al. 2006) the strength of the simulated present-day AMOC in different CGCMs varies substantially. While the CCC CGCM2 has a mean overturning strength of 14 Sv, the GFDL CM2.1 has a magnitude of 24 Sv. As explained above, these differences may also translate into differences in the simulation of tropical Pacific climate, including the cold tongue, the

annual cycle, ENSO and ENSO decadal variability. Systematic biases in the Pacific may be related to systematic modeling biases in the Atlantic. Further research has to be done to understand these SST bias teleconnections between the ocean basins.

We are aware that our study raises probably more questions than it answers. Questions to be addressed in future research are:

- How exactly does the nonlinear frequency entrainment mechanism for ENSO work physically?
- Why is there such an inconsistency between model for the simulated Pacific thermocline depth anomalies?
- What is the role of topographic features in Central America to link northern tropical Atlantic SST anomalies with the tropical Pacific climate?

Further research needs to be done to translate the results from this study into a better understanding of ENSO's multidecadal variabilty and its sensitivity to a future weakening of the AMOC as projected by some CGCMs (Schmittner et al. 2005).

Acknowledgments A. Timmermann, and S.-P. Xie are supported by the Japan Agency for Marine-Earth Science and Technology (JAMSTEC) through its sponsorship of the International Pacific Research Center. T.F. Stocker was partly supported by the IPRC visitor program. A.C. received funding from the NSF Paleoclimate program ATM0134742. The support of the European Union's Framework Programme VI via the DYNAMITE project (contract 003903) is also acknowledged. SIA was supported by grant No. R01-2006-000-10441-0 from the Basic Research Program of the Korea Science and Engineering Foundation and the Brain Korea 21 project. CCSM3 simulations were performed at CSCS Manno. TFS and MR acknowledge support by the Swiss National Science Foundarion through NCCR Climate. We thank Tony Broccoli, Andrew Wittenberg and Rich Gudgel for the constructive comments on an earlier version of the manuscript.

References

Arnol'd, V., 1965: Small denominators. I Mappings of the circumference onto itself. *Am. Math. Soc. Trans.*, **46**, 213–284.

Bak, P., T. Bohr, and M. Jensen, 1985: Mode locking and the transition to chaos in dissipative systems. *Physica Scripta*, **T9**, 50–58.

Black, D., L. Peterson, J. Overpeck, A. Kaplan, M. Evans, and M. Kashgara-

ian, 1999: Eight centuries of north atlantic ocean atmosphere variability. *Science*, **286**, 1709–1713.

Blunier, T., J. Chappellaz, J. Schwander, A. Dällenbach, B. Stauffer, T. F. Stocker, D. Raynaud, J. Jouzel, H. Clausen, C. Hammer, and S. Johnsen, 1998: Asynchrony of Antarctica and Greenland during the last glacial. *Nature*, **394**, 739–743.

Broccoli, A., K. Dahl, and R. Stouffer, 2006: Response of the ITCZ to Northern Hemisphere cooling. *Geophys. Res. Lett.*, L01702, doi:10.1029/2005GL024546.

Cessi, P., K. Bryan, and R. Zhang, 2004: Global seiching of thermocline waters between the Atlantic and the Indian-Pacific Ocean Basins. *Geophys. Res. Lett.*, **31**, doi: 10.1029/2003GL019091.

Chang, P., B. Wang, T. Li, and L. Ji, 1994: Interactions between the seasonal cycle and the southern oscillation - frequency entrainment and chaos in a coupled ocean-atmosphere model. *Geophys. Res. Lett.*, **21**, 2817–2820.

Chiang, J. and C. Bitz, 2005: Influence of high latitude ice cover on the marine Intertropical Convergence Zone. *Clim. Dyn.*, **25**, 477–496, doi: 10.1007/s00382–005–0040–5.

Clement, A. C., R. Seager, and M. A. Cane, 1999: Orbital controls on the tropical climate. *Paleoceanography*, **14**, 441–456.

Collins, M. and the CMIP Modelling Groups, 2005: El Niño- or La Niña-like climate change? *Clim. Dyn.*, **24**, 89–104.

Corrège, T., T. Delcroix, J. Récy, W. Beck, G. Cabioch, and F. L. Cornec, 2000: Evidence for stronger El Niño-Southern Oscillation (ENSO) events in a mid-Holocene massive coral. *Paleoceanogr.*, **15**, 465–470.

Dahl, K. A., A. J. Broccoli, and R. J. Stouffer, 2005: Assessing the role of North Atlantic freshwater forcing in millennial scale climate variability: a tropical Atlantic perspective. *Climate Dynamics*, **24**, 325–346.

Delworth, T. and et al., 2006: GFDLs CM2 global coupled climate models. Part I: Formulation and simulation characteristics. *J. Climate*, 643–674.

Delworth, T., S. Manabe, and R. Stouffer, 1993: Interdecadal variations of the thermohaline circulation in a coupled ocean-atmosphere model. *J. Climate*, **6**, 1900–1989.

Delworth, T. and M. Mann, 2000: Observed and simulated multidecadal variability in the northern hemisphere. . *Clim. Dyn.*, **16**, 661–676.

Dixon, K., T. Delworth, M. Spelman, and R. Stouffer, 1999: The influence of transient surface fluxes on North Atlantic overturning in a coupled climate change experiment. *Geophys. Res. Lett.*, **26**, 2749–2752.

Dong, B. and R. Sutton, 2002: Adjustment of the coupled ocean-

atmosphere system to a sudden change in the Thermohaline Circulation. *Geophys. Res. Lett.*, **29**, 10.129/2002GL015229.

Dong, B.-W., R. Sutton, and A. Scaife, 2006: Multidecadal modulation of El Nino-Southern Oscillation (ENSO) variance by Atlantic Ocean sea surface temperatures. *Geophys. Res. Lett*, **33**, L08705, doi:10.1029/2006GL025766.

Ducet, N., P. L. Traon, and G. Reverdin, 2000: Global high resolution mapping of ocean circulation from TOPEX/Poseidon and ERS-1/2. *J. Geophys. Res.*, **105**, 19477–19498.

Eisenman, I., L. Yu, and E. Tziperman, 2005: Westerly Wind Bursts: ENSO's tail rather than the dog. *J. Climate*, **18**, 5224–5238.

Fedorov, A. V. and S. Philander, 2000: Is El Niño changing? *Science*, **288**, 1997–2002.

Galanti, E., E. Tziperman, M. Harrison, A. Rosati, R. Giering, and Z. Sirkes, 2002: he equatorial thermocline outcropping: A seasonal control on the tropical pacific ocean- atmosphere instability strength. *J. Climate*, **15**, 2721–2739.

Gill, A., 1980: Some simple solutions for heat induced tropical circulation. *Quart. J. Roy. Meteor. Soc.*, **106**, 447–462.

Gnanadesikan, A. and et al., 2006: GFDL's CM2 Global Coupled Climate Models. Part II: The Baseline Ocean Simulation. *J. Climate*, **19**, 675–669.

Goodman, P. J., 2001: Thermohaline Adjustment and Advection in an OGCM. *J. Phys. Oceanogr.*, **31**, 1477–1497.

Gordon, C., C. Cooper, C. Senior, H. Banks, J. Gregory, T. Johns, J. Mitchell, and R. Wood, 2000: The simulation of SST, sea ice extents and ocean heat transports in a version of the Hadley Centre coupled model without flux adjustments. *Clim. Dyn.*, **16**, 147–168.

Gregory, J. and et al., 2005: A model intercomparison of changes in the Atlantic thermohaline circulation in response to increasing CO_2 concentration. *Geophys. Res. Lett.*, **32**, L12703,doi:10.1029/2005GL023209.

Griffies, S. and K. Bryan, 1997: A predictability of simulated North Atlantic multidecadal variability. *Clim. Dyn.*, **13**, 459–487.

Griffies, S. and et al., 2006: Formulation of an ocean model for global climate simulation. *Ocean Science*, **1**, 45–79.

Grötzner, A., M. Latif, A. Timmermann, and R. Voss, 1999: Interannual to Decadal Predictability in a Coupled Ocean-Atmosphere General Circulation Model. *J. Climate*, **12**, 2607–2624.

Gu, D. and S. Philander, 1995: Secular changes of annual and interannual variability in the tropics during the past century. *J. Clim.*, **8**, 864–876.

Guilyardi, E., 2005: El Niño-mean state-seasonal cycle interactions in a multi-model ensemble. *Clim. Dyn*, DOI: 10.1007/s00382–005–0084–6.

Hemming, S., 2004: Heinrich events: Massive late Pleistocene detritus layers of the North Atlantic and their global climate imprint. *Rev. in Geophys.*, **42**, RG1005.

Hsieh, W. and K. Bryan, 1996: Redistribution of sea level rise associated with enhanced greenhouse warming: a simple model study. *Clim. Dyn.*, **12**, 535–544.

Huang, R., M. Cane, N. Naik, and P. Goodman, 2000: Global adjustment of the thermocline in response to deepwater formation. *Geophys. Res. Lett.*, **27**, 759–762.

Huygens, C., 1669: Instructions concerning the use of pendulum-watches, for finding the Longitude at Sea. *Philos. Trans. Royal Soc.*, **4**, 937.

Ivanochko, T., R. Ganeshram, G.-J. Brummer, G. Ganssen, S. Jung, S. Moreton, and D. Kroon, 2005: Variations in Tropical Convection as an Amplifier of Global Climate Change at the Millennial Scale. *Earth. Planet. Sci. Lett.*, **235**, 302–314.

Jin, F.-F., L. Lin, A. Timmermann, and J. Zhao, 2006: Ensemble-mean dynamics of the enso recharge oscillator under state-dependent stochastic forcing. *Geophys. Res. Lett.*, accepted.

Johnson, H. and D. Marshall, 2004: Global Teleconnections of Meridional Overturning Circulation Anomalies. *J. Phys. Oceanogr.*, **34**, 1702–1722.

Jungclaus, J., M. Botzet, H. Hakk, N. Keenlyside, J.-J. Luo, M. Latif, J. Marotzke, U. Mikolajewicz, and E. Roeckner, 2006: Ocean circulation and tropical variability in the coupled model ECHAM5/MPI-OM. *J. Climate*, **19**, 3952–3972.

Kalnay, E. and et al., 1996: The NCEP/NCAR 40-year reanalysis project. *Bull. Amer. Meteor. Soc.*, **77**, 437–471.

Kerr, R., 2000: A North Atlantic climate pacemaker for the centuries. *Science*, **288**, 1984–1985.

Kiehl, J. and P. Gent, 2004: The Community Cimate System Model, version two. *J. Climate*, **17**, 3666–3682.

Knutson, T., S. Manabe, and D.-F. Gu, 1997: Simulated ENSO in a global coupled ocean-atmosphere model: multi-decadal amplitude modulation and CO_2 sensitivity. *J. Climate*, **10**, 138–161.

Knutti, R., J. Flückiger, T. Stocker, and A. Timmermann, 2004: Strong hemispheric coupling of glacial climate through freshwater discharge and ocean circulation. *Nature*, **430**, 851–856.

Koutavas, A. and J. Lynch-Stieglitz: 2004, *The Hadley circulation: Present,*

Past and Future, Springer, New York, chapter Variability of the marine ITCZ over the easten Pacific during the past 30,000 years. 347–369.

Kraus, E. and J. Turner, 1967: A one dimensional model of the seasonal thermocline. Part II. *Tellus*, **19**, 98–105.

Latif, M., M. Collins, H. Pohlmann, and N. Keenlyside, 2006: The physical basis for prediction of Atlantic sector climate on decadal timescales. *J. Climate*, in press.

Lea, D., D. Pak, L. Peterson, and K. Hughen, 2003: Synchroneity of tropical and high-latitude atlantic temperatures over the last glacial termination. *Science*, **301**, 1361 – 1364.

Levitus, S., 1994: Climatological Atlas of the World Ocean. Technical report, NOAA Prof. Paper 13.

Li, T. and S. G. H. Philander, 1996: On the Annual Cycle of the Equatorial Eastern Pacific. *J. Clim.*, **9**, 2986–2998.

Liu, Z., 2002: A simple model study of the forced response of ENSO to an external periodic forcing. *J. Clim.*, **15**, 1088–1098.

Manabe, S. and R. Stouffer, 1988: Two Stable Equilibria of a Coupled Ocean-Atmosphere Model. *J. Climate*.

Marsland, S., H. Haak, J. Jungclaus, M. Latif, and F. Röske, 2003: The Max-Planck-Institute global ocean/sea ice model with orthogonal curvilinear coordinates. *Ocean Modelling*.

Meehl, G., C. Covey, B. McAvaney, M. Latif, and R. Stouffer, 2005: Overview of the coupled model intercomparison project. *Bulletin of the American Meteorological Society*, **86**, 89–93.

Merryfield, W., 2006: Changes to ENSO under CO_2 doubling in a multi-model ensemble. *J. Climate*, in press.

Pacanowski, R. and S. Philander, 1981: Parameterization of vertical mixing in mumerical models of tropical oceans. *J. Phys. Oceanogr.*, **11**, 1443–1451.

Peterson, L., G. Haug, K. Hughen, and U. Rohl, 2000: Rapid changes in the hydrologic cycle of the tropical Atlantic during the last glacial. *Science*, **290**, 1947–1951.

Philander, S., D. Gu, D. Halpern, G. Lambert, N.-C. Lau, T. Li, and R. Pacanowski, 1996: Why the ITCZ is mostly north of the equator. *J. Climate*, **9**, 2958–2972.

Philip, S. and G. van Oldenborgh, 2006: Shifts in ENSO coupling processes under global warming. *Geophys. Res. Let.*., accepeted.

Pikovsky, A., M. Rosenblum, and J. Kurths, 2000: Phase synchronization in regular and chaotic systems. *Int. J. of Bifurcation and Chaos*, **10**.

Rayner, N., D. Parker, E. Horton, C. Folland, L. Alexander, D. Rowell, E. Kent, and A. Kaplan, 2003: Global analyses of sea surface temperature, sea ice, and night marine air temperature since the late nineteenth century. *J. Geophys. Res.*, **108**, 4407, doi:10.1029/2002JD002670.

Rein, B., A. Lückge, L. Reinhardt, F. Sirocko, A. Wolf, and W.-C. Dullo, 2005: El Niño variability off Peru during the last 20,000 years. *Paleoceanography*, **20**, PA4003,doi:10.1029/2004PA001099.

Reynolds, R., N. Rayner, T. Smoth, D. Stokes, and W. Wang, 2002: An improved in situ and satellite SST analysis for climate. *J. Climate*, **15**, 1609–1625.

Roeckner, E., G. Bäuml, L. Bonaventura, R. Brokopf, M. Esch, M. Giorgetta, S. Hagemann, I. Kirchner, L. Kornblueh, E. Manzini, A. Rhodin, U. Schlese, U. Schulzweida, and A. Tompkins, 2003: The atmospheric general circulation model ECHAM5, part I: Model description. Technical Report 349, Max- Planck- Institut für Meteorologie.

Schmittner, A., M. Latif, and B. Schneider, 2005: Model Projections of the North Atlantic thermohaline circulation for the 21st century assessed by observations. *Geophys. Res. Lett.*, **32**.

Seo, H., M. Jochum, R. Murtugudde, and A. Miller, 2006: Effect of ocean mesoscale variability on the mean state of tropical Atlantic climate. *Geophys. Res. Lett.*, **33**, L09606, doi: 10.1029/2005GL025651.

Stocker, T. F. and S. Johnsen, 2003: A minimum thermodynamic model for the bipolar seesaw. *Paleoceanography*, **18**, 1087, doi:10.1029/2003PA000920.

Stott, L., C. Poulsen, S. Lund, and R. Thunell, 2002: Super ENSO and Global Climate Oscillations at Millenial Time Scales. *Science*, **297**, 222–226.

Stouffer, R., J. Yin, J. Gregory, K. Dixon, M. Spelman, W. Hurlin, A. Weaver, M. Eby, G. Flato, H. Hasumi, A. Hu, J. Jungclaus, I. Kamenkovich, A. Levermann, M. Montoya, S. Murakamiu, S. Nawrath, A. Oka, W. Peltier, D. Robitaille, A. Sokolov, G. Vettoretti, S. W. Stouffer, J. Yin, J. Gregory, and et al., 2006: Investigating the causes of the response of the thermohaline circulation to past and future climate changes . *J. Climate*, **19**, 1365–1387.

Timmermann, A., 2003: Decadal ENSO Amplitude Modulations: A Nonlinear Mechanism. *Glob. Planet. Changes*, **37**, 135–156.

Timmermann, A., S. An, U. Krebs, and H. Goosse, 2005a: ENSO suppression due to a weakening of the North Atlantic thermohaline circulation. *J. Climate*, **18**, 3122–3139.

Timmermann, A. and F.-F. Jin: 2006, *Predictability of Weather and Climate*, Cambridge University Press, UK, chapter Predictability of coupled processes. 251–274.

Timmermann, A., Krebs, F. Justino, H. Goosse, and T. Ivanochko, 2005b: Mechanisms for millennial-scale global synchronization during the last glacial period . *Paleoceanography*, **20**, PA4008, doi: 10.1029/2004PA00109.

Timmermann, A., M. Latif, A. Bacher, J. Oberhuber, and E. Roeckner, 1999a: Increased El Niño frequency in a climate model forced by future greenhouse warming. *Nature*, **398**, 694–696.

Timmermann, A., M. Latif, and R. Voss, 1999b: Modes of Climate Variability as simulated by the coupled atmosphere-ocean model ECHAM3/LSG, Part I: ENSO-like climate variability and its low-frequency modulation. *Climate Dyn.*, **15**, 605–618.

Timmermann, A., M. Latif, R. Voss, and A. Grötzner, 1998: Northern Hemispheric Interdecadal Variability: A coupled Air-Sea Mode. *J. Climate*, **11**, 1906–1931.

Timmermann, A., S. Lorenz, S.-I. An, A. Clement, and S.-P. Xie, 2006: The effect of orbital forcing on the mean climate and variability of the tropical Pacific. *J. Climate*, submitted.

Tudhope, A., C. P. Chilcott, M. McCulloch, E. Cook, J. Chappell, R. Ellam, D. Lea, J. Lough, and G. Shimmield, 2001: Variability in the El Niño-Southern Oscillation Through a Glacial-Interglacial Cycle. *Science*, **291**, 1511–1517.

Tziperman, E., L. Stone, M. Cane, and H. Jarosh, 1994: El Niño Chaos: Overlapping of Resonances Between the Seasonal Cycle and the Pacific Ocean-Atmosphere Oscillator. *Science*, **264**, 72.

Tziperman, E., S. Zebiak, and M. Cane, 1997: Mechanisms of Seasonal – ENSO Interaction. *J. Atmos. Scien.*, **54**, 61–71.

Vellinga, M., R. Wood, and J. M. Gregory, 2001: Processes Governing the Recovery of a Perturbed Thermohaline Circulation in HadCM3. *J. Climate*, **15**, 764–779.

Wang, B., R. Wu, and R. Lukas, 2000: Annual Adjustment of the Thermocline in the Tropical Pacific Ocean. *J. Climate*, **13**, 596–616.

Wang, Y., S.-P. Xie, H. Xu, and B. Wang, 1999: Regional Model Simulations of Marine Boundary Layer Clouds over the Southeast Pacific off South America, Part I: Control Experiment. *Mon. Wea. Rev.*, 274–296.

Wittenberg, A. and et al., 2006: GFDL's CM2 Global Coupled Climate Models. Part III: Tropical Pacific Climate and ENSO. *J. Climate*, in press.

Wright, D., 1997: A new eddy mixing parametrization and ocean general circulation model. *International WOCE newsletter*, **26**, 27–29.

Wu, L., F. He, and Z. Liu, 2005: Coupled Ocean-Atmosphere Response to North Tropical Atlantic SST: tropical Atlantic Dipole and ENSO. *Geophys. Res. Lett.*, **32**.

Xie, S.-P., 1994: On the Genesis of the Equatorial Annual Cycle. *J. Clim.*, **7**, 2008–2013.

— 1996: Effects of Seasonal Forcing on Latitudinal Asymmetry of the ITCZ. *J. Climate*, **9**, 2945–2950.

Xie, S.-P., T. Miyama, Y. Wang, H. Xu, S. deSzoeke, R. Small, K. Richards, T. Mochizuki, and T. Awaji, 2006: A Regional Ocean-Atmophere Model for Eastern Pacific Climate: Towards Reducing Tropical Biases. *J. Climate*, submitted.

Yeager, S., C. Shields, W. Large, and J. Hack, 2006: The low resolution CCSM3. *J. Climate*, **19**, 2545–2566.

Yu, J.-Y. and C. Mechoso, 1999: Links between annual variations of Peruvian stratocumulus clouds and of SST in the eastern equatorial Pacific. *J. Climate*, **12**, 3305–3318.

Zebiak, S. E. and M. A. Cane, 1987: A model El Niño-Southern Oscillation. *Month. Weath. Rev.*, **115**, 2262–2278.

Zhang, R. and T. Delworth, 2005: Simulated Tropical Response to a Substantial Weakening of the Atlantic Thermohaline Circulation. *J. Climate*, **18**, 1853–1860.

List of Figures

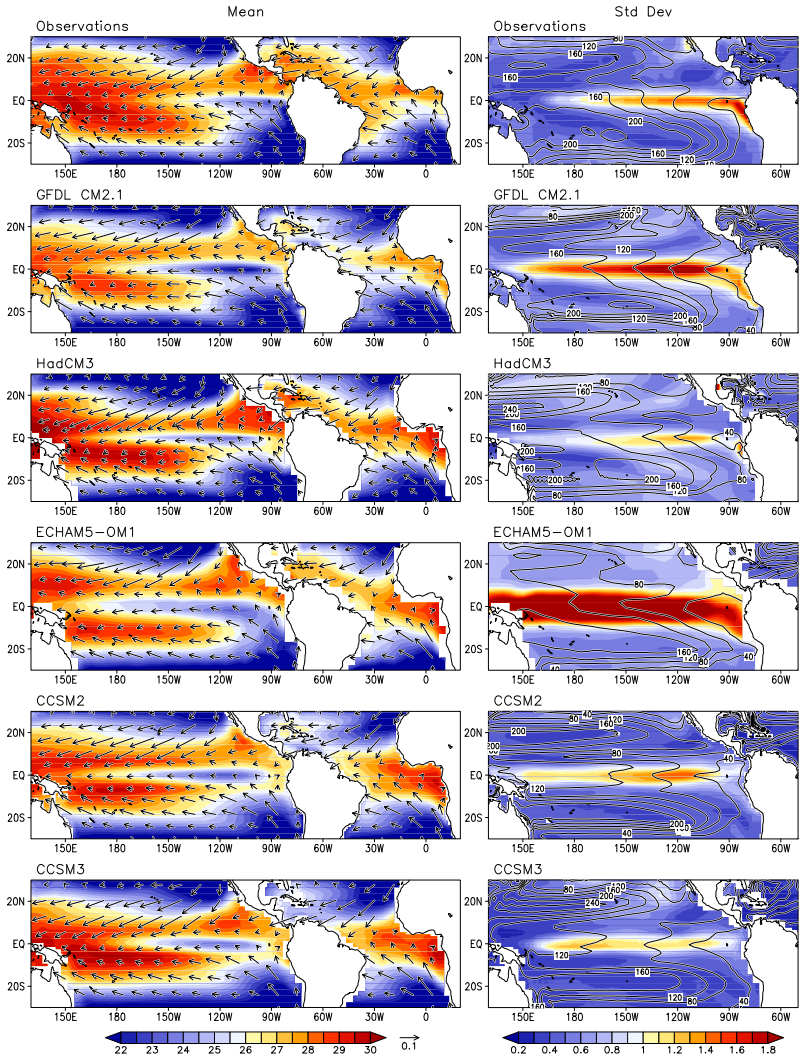

Figure 1: Left panels: observed longterm annual mean SST (Reynolds et al. 2002) [°C] (averaged from December 1981 - December 2005) and wind stress (Kalnay and et al. 1996) [Nm^{-2}] (averaged from January 1948 - March 2005), simulated annual mean SST for the GFDL CM2.1 (pre-industrial), the HadCM3 model (pre-industrial), the MPI-OM1 (pre-industrial), the NCAR CCSM2 (present-day) andthe NCAR CCSM3 (present-day) model. Right panels: Same as left panel but for the longterm annual mean thermocline depth Levitus (1994) [m] (contours) and the standard deviation of SST anomalies [K].

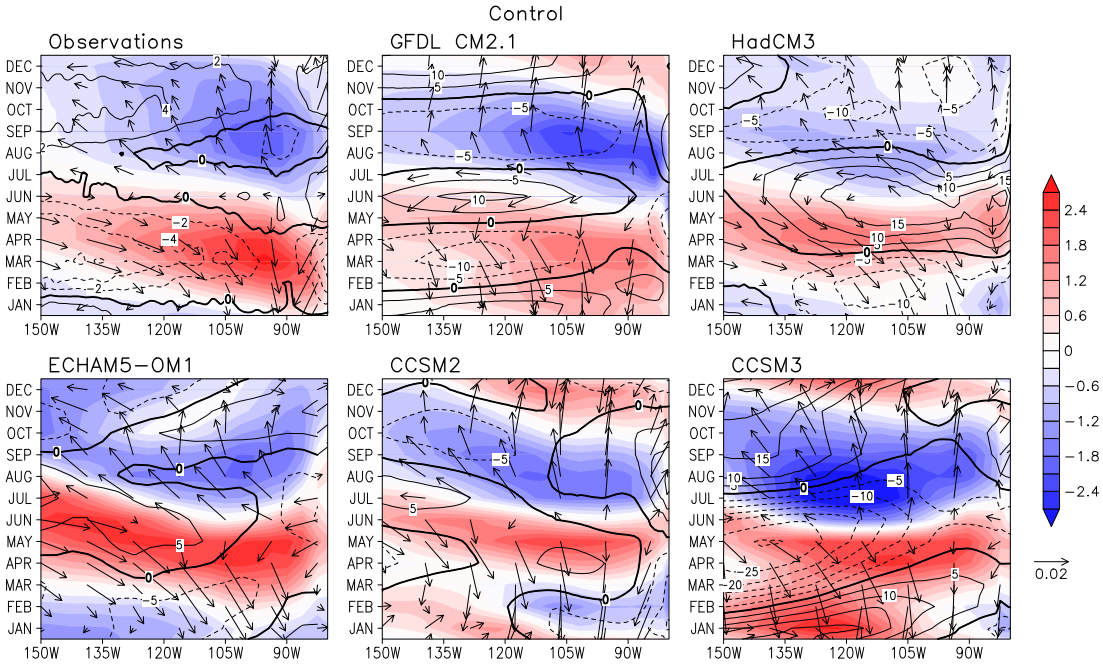

Figure 2: Hovmoller diagrams of the mean present-day seasonal cycle of Pacific equatorial SST (shading) using the observed SST (Reynolds et al. 2002), wind stress (Kalnay and et al. 1996) and sea level data (Ducet et al. 2000). A 1 cm increase in sea surface height roughly corresponds to a 3-m deepening of the thermocline (assuming a 1.5-layer model with a reduced gravity of 0.003 kg/m^3.) Hovmoller diagrams of the the simulated SST, wind stress and thermocline depth (depth of the 20°C isotherm in contours) climatologies obtained from the first 100 years of the control simulations of the GFDL CM2.1 (pre-industrial), the HadCM3 (pre-industrial), the MPI-OM1 (pre-industrial), the CCSM2 (present-day) and CCSM3 (present-day) models.

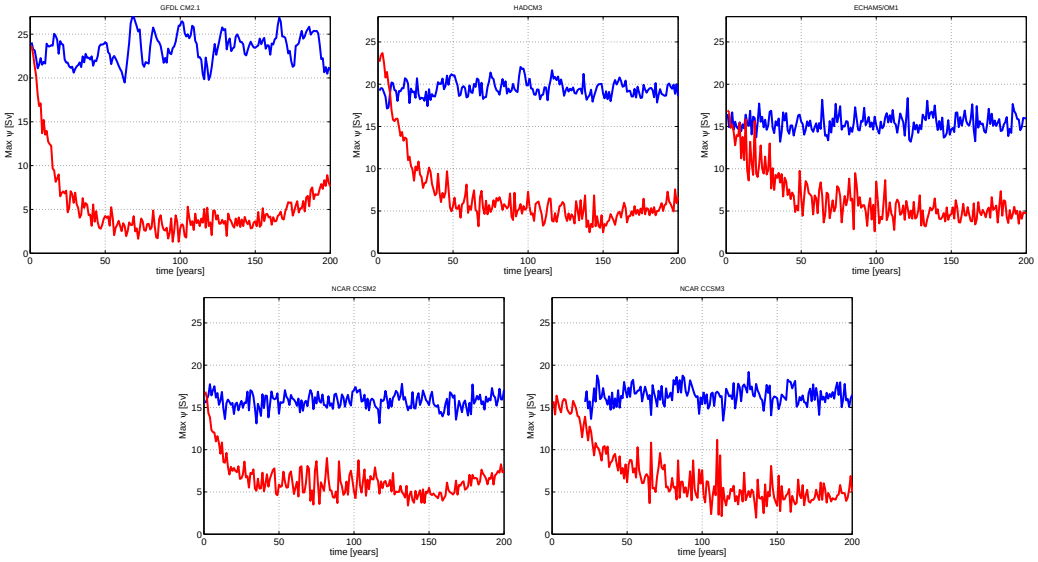

Figure 3: Timeseries of the maximum of the meridional streamfunction in the North Atlantic [1 Sv= 10^6 m^3/s] for the five different models and the waterhosing experiment (red) and the control experiment (blue). The initial states for the waterhosing experiments are obtained from different stages of the respective control simulations.

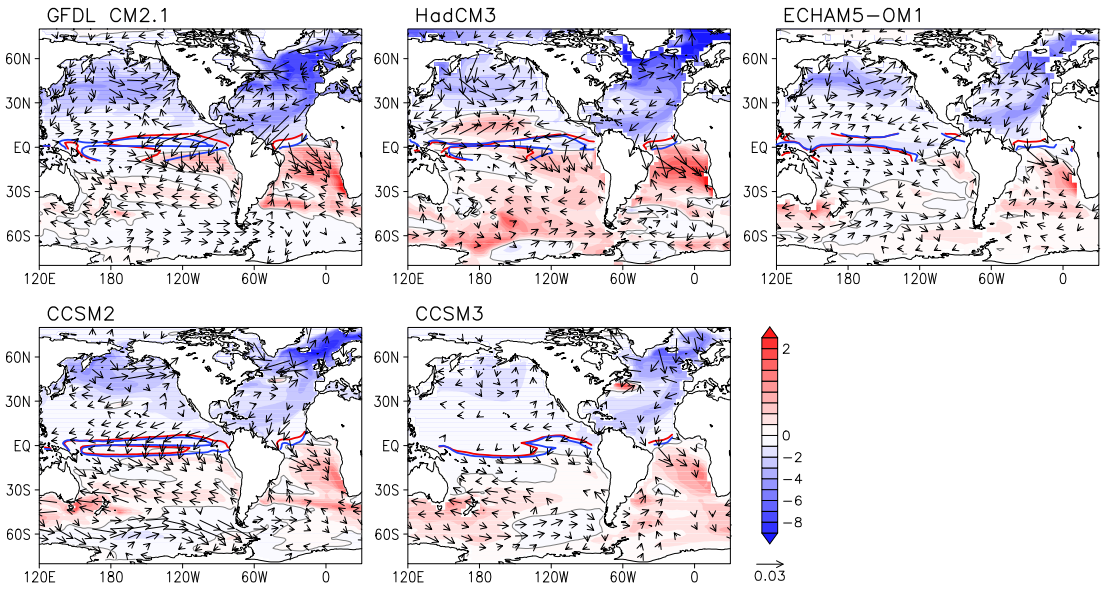

Figure 4: SST anomaly [K] and wind stress anomaly [N/m^2] generated by the shutdown of the AMOC for the GFDL CM2.1 model (upper left), the HadCM3 (upper middle), the MPI-OM1 (upper right), the CCSM2 model(lower left), and the CCSM3 model (lower right). The red, blue lines represent the annual mean $\tau_y = 0$ lines in the control and waterhosing experiment, respectively. Note the asymmetric temperature scale.

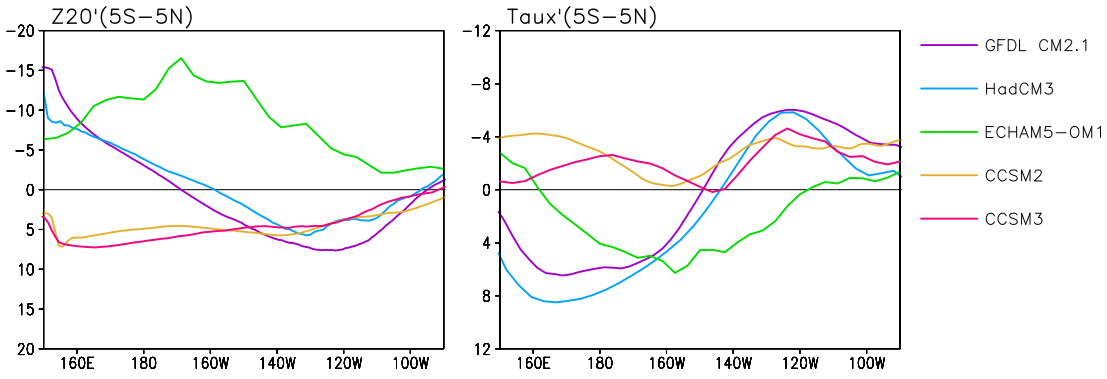

Figure 5: Thermocline depth anomalies [m] (left) and wind stress anomalies associated with a the perturbation state of the AMOC (averaged difference between 200 model years of the waterhosing experiment and the control run). The anomalies are computed as the spatial avagerage between 5°S and 5°N for the GFDL CM2.1 (purple), the HadCM3 (blue), the MPI-OM1 (green), the CCSM2 (yellow) and the CCSM3 (magenta) models. Positive thermocline depth anomalies represent a deepening of the thermocline.

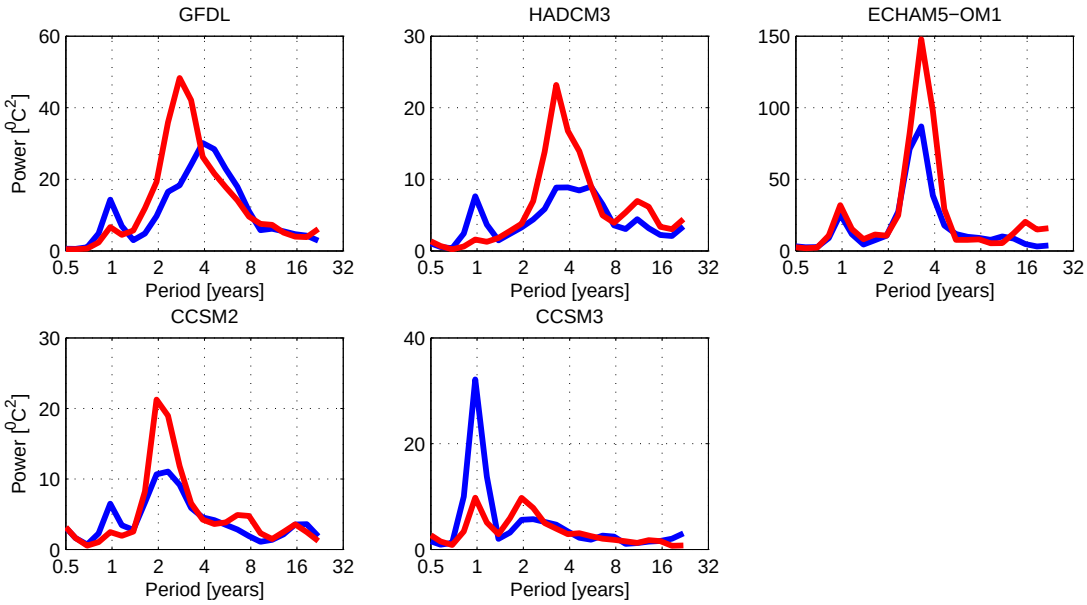

Figure 6: Power spectra of the simulated Niño 3 SSTA for the GFDL CM2.1 model (upper left), the HadCM3 model (upper middle), the MPI-OM1 (upper right), the CCSM2 model (lower left) and the CCSM3 model (lower middle). The Niño 3 SSTA is obtained by averaging the monthly SST over the region 90°W-150°W, 5°S-5°N and by subtracting only the long term annual mean, thereby retaining also seasonal variability. The power spectra of the Niño 3 SSTA for control run (first 200 years) are shown in blue, while the ones for the water hosing experiments (first 200 years) are depicted in red.

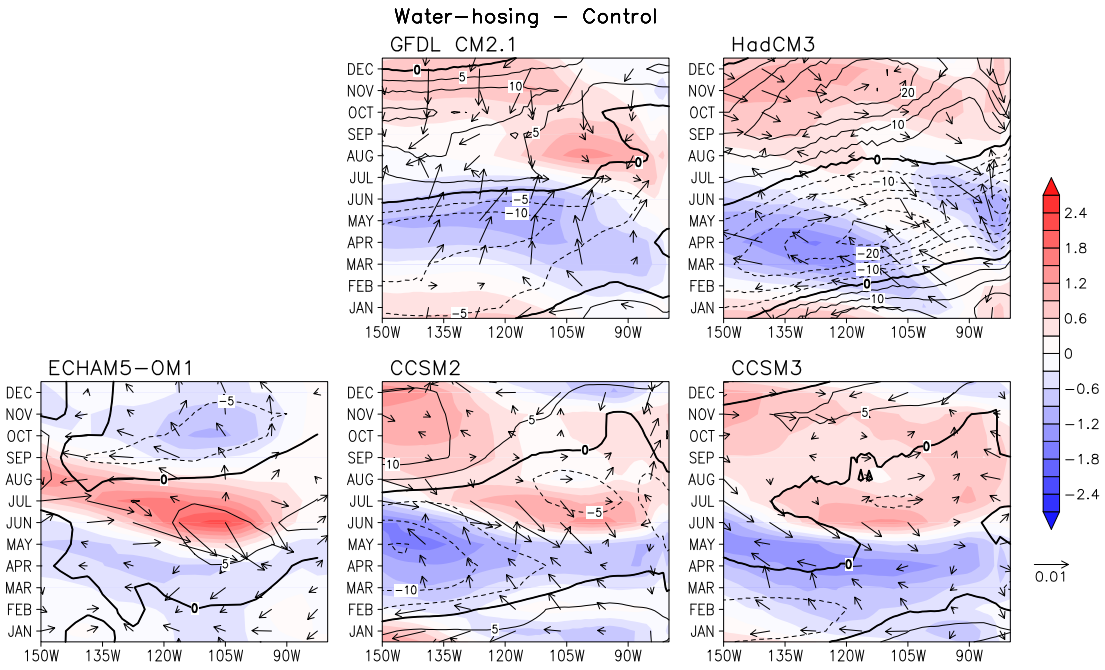

Figure 7: Left: Hovmoller diagram of difference of the simulated equatorial mean seasonal cycle of SST (shading), wind stress (vector) and thermocline depth (contour) in the waterhosing experiment (average over first 100 years) and the control simulation (first 100 years).The annual mean difference of the respective fields were removed prior to the analysis.

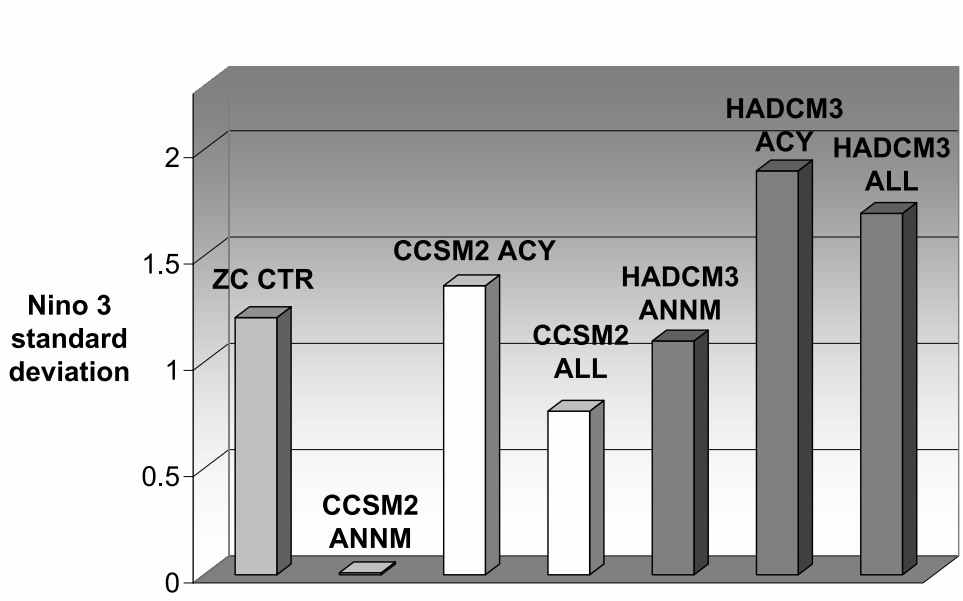

Figure 8: Standard deviation of simulated Niño 3 SSTA [K] using the ZC model background state (ZC CTR) plus: the annual mean anomaly of the CCSM2 waterhosing eperiment of wind, thermocline and SST (CCSM2 ANNM); the anomalous seasonal cycle of the CCSM2 waterhosing eperiment of wind, thermocline and SST (CCSM2 ACY); the anomalous seasonal cycle plus background state of the CCSM2 waterhosing eperiment of wind, thermocline and SST (CCSM2 ALL); the annual mean anomaly of the HadCM3 waterhosing eperiment of thermocline depth only (HADCM3 ANNM); the anomalous seasonal cycle of the HADCM3 waterhosing eperiment of thermocline depth only (HADCM3 ACY); the anomalous seasonal cycle plus background state of the HADCM3 waterhosing eperiment of thermocline depth only (HADCM3 ALL).

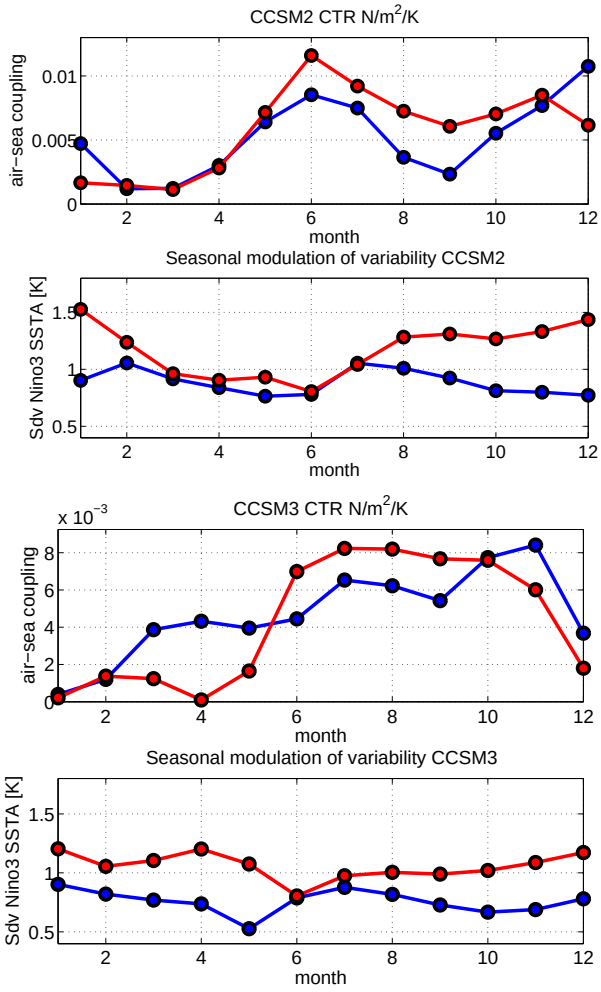

Figure 9: Upper panels: monthly regression between zonal wind-stress in the central Pacific (averaged over 170°E-140°W and 5°S-5°N) and the Niño3 SSTA obtained from the CCSM2 and CCSM3 models. Unit is Pa/K.Lower panels: monthly standard deviation of the Niño3 SSTA. Blue curves represent the first 100 years of the control simulation. Red curves are obtained from the first 100 years of the waterhosing experiments.

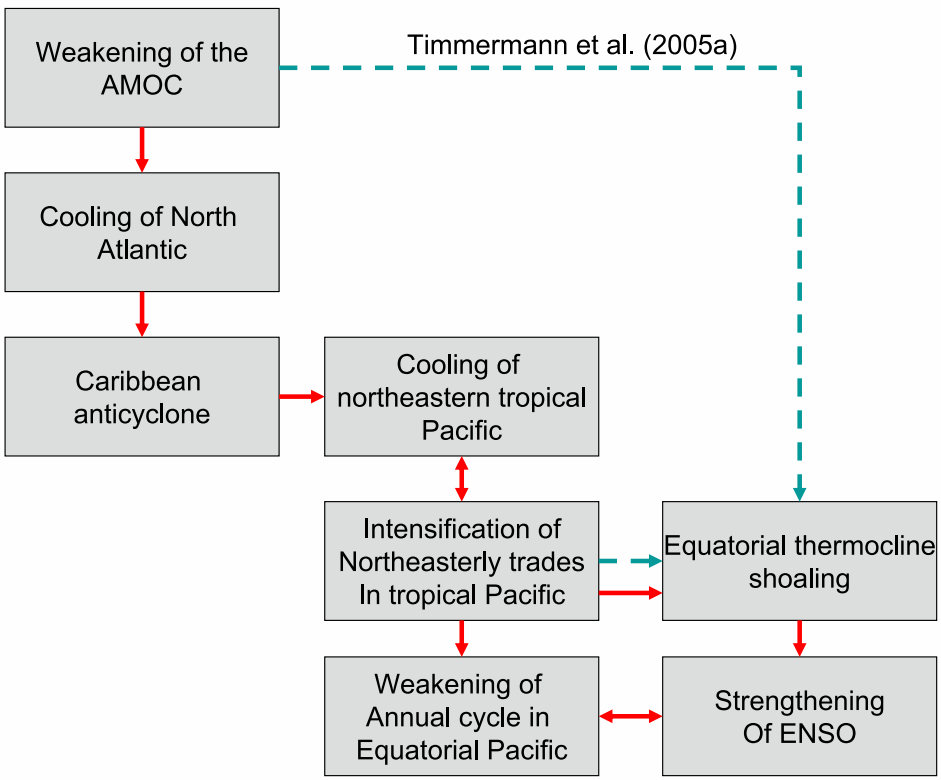

Figure 10: Schematic illustration of the influence of shutdown of the AMOC on the mean state of the eastern equatorial Pacific, the annual cycle and ENSO. Solid lines represent a positive correlation, while dashed lines represent a negative relationship.

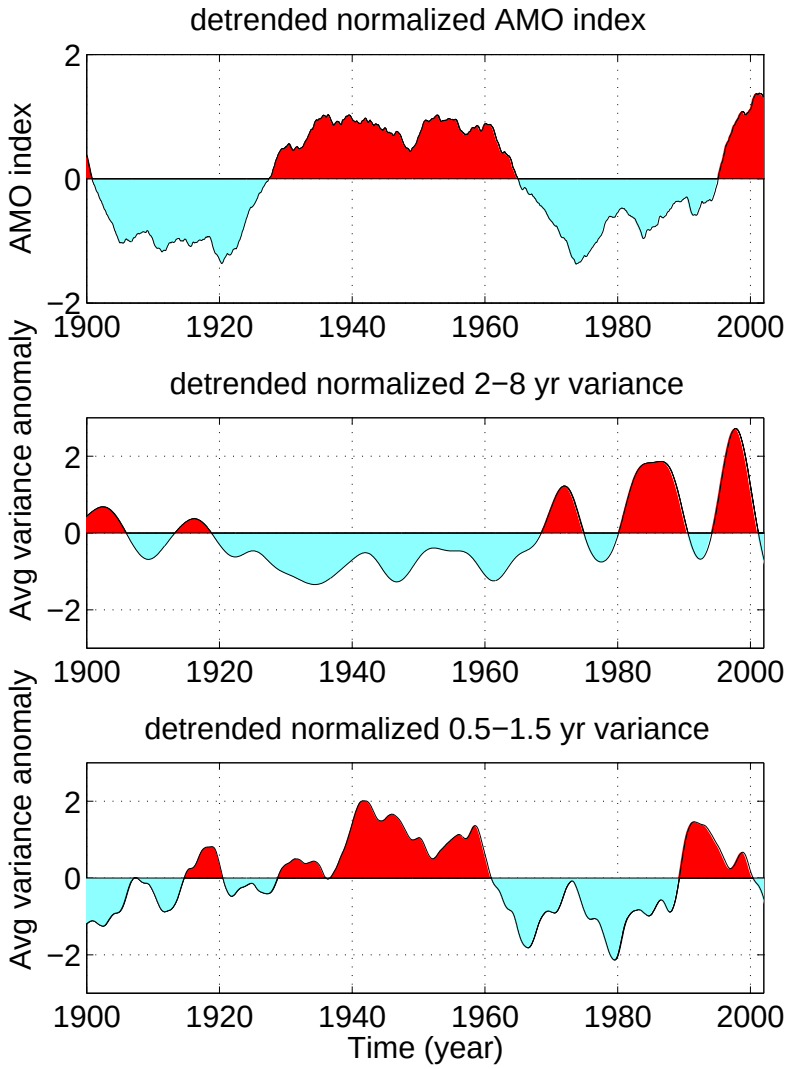

Figure 11: Upper: Low-pass filtered and detrended observed AMO SST index and observed annual and interannual variance anomaly of Niño 3 SSTA, obtained from the wavelet variance integrated over the periodicity bands 2–8 years and 0.5–1.5 years, respectively. All time-series were normalized by their respective standard deviations. The AMO index was calculated by averaging annual mean SST observations (Rayner et al. 2003) over the North Atlantic region 0°-60° and 75°W-7.5°W

List of Tables

Model	Atmosphere res.	Ocean res.	CO_2 [ppmv]	Niño 3 SST [K]
GFDL CM2.1	2x2.5, L24	1/3-1x1, L50 (MOM4)	286	1.59
HadCM3	2.5x3.75, L19	1.25x1.25, L20	290	1.05
CCSM2	T42, L26	1x1, L40 (POP)	354	1.21
CCSM3	T31	3.75x1.8 - 3.75x0.9, L25	354	1.55
ECHAM5-OM1	T31, L19	3x3	280	2.21

Table 1: Summary of Coupled General Circulation Models used in this study and their simulated standard deviation of Niño 3 SST (including annual cycle). The observed Niño SST standard deviation is 1.25 K (averaged from 1960 to 2006).